Collective molecular-scale carbonation path in aqueous solutions with sufficient structural sampling: From CO2 to CaCO3

Xinping Zhu, Romain Dupuis, Roland J.-M. Pellenq, Katerina Ioannidou

Collective molecular-scale carbonation path in aqueous solutions with sufficient structural sampling: from CO_2 to $CaCO_3$

Xinping Zhu, Romain Dupuis, and Katerina Ioannidou
Laboratoire de Mécanique et Génie Civil (LMGC), CNRS, Université de Montpellier, Montpellier, France

Roland J-M Pellenq
Institut Européen des Membranes (IEM), CNRS, Université de Montpellier, Montpellier, France
(*aikaterini.ioannidou@umontpellier.fr)
(*roland.pellenq@cnrs.fr)
(Dated: January 6, 2025)

Carbonation reaction is essential in the global carbon cycle and in the carbon dioxide (CO_2) capture. In oceans (pH 8.1) or in synthetic materials such as cement or geopolymers (pH over 12), the basic pH conditions affect the reaction rate of carbonation. However, the precipitation of calcium or magnesium carbonates acidifies the environment and, therefore, limits further CO_2 capture. Herein, we investigate how pH influences carbonation pathways in neutral and basic solutions at the atomic scale using reactive molecular simulations coupled with enhanced sampling methods from CO_2 to calcium carbonate ($CaCO_3$). Two distinct CO_2 conversion pathways are identified:(1) CO_2 hydration: $CO_2 + H_2O \rightleftharpoons H_2CO_3 \rightleftharpoons HCO_3^- + H^+ \rightleftharpoons CO_3^{2-} + 2H^+$; (2) CO_2 hydroxylation: $CO_2 + OH^- \rightleftharpoons HCO_3^- \rightleftharpoons CO_3^{2-} + H^+$. The CO_2 hydration pathway occurs in both neutral and basic aqueous solutions, but reactions differ significantly between the two pH conditions. The formation of the CO_3^{2-} is characterized by a markedly high free energy barrier in the neutral solution. The CO_2 hydroxylation pathway is only found in basic solutions. Notably, the CO_2 molecule exhibits a pronounced energetic preference for reacting with hydroxide ions (OH^-) rather than with water molecules, resulting in significantly reduced free energy barriers along the CO_2 hydroxylation pathway. The reaction rate estimation suggests that the CO_2 hydroxylation path is the most favorable carbonation pathway in the basic solution. Once the CO_3^{2-} anion is formed in the presence of alkali-earth (e.g., Ca^{2+} and Mg^{2+}) cation, carbonate formation can proceed.

I. INTRODUCTION

The global concentration of atmospheric carbon dioxide (CO_2) at present is about 418 ppm, the highest level in mankind history [1]. To mitigate this, it is continuously increasing by around 2.3 ppm per year. To this end, innovative carbon capture and sequestration technologies have been developed, particularly the CO_2 mineralization-related methods that can be widely used in large-scale geological sequestration using industrial flue gas [2–4]. Seas and oceans also act as a gigantic carbon sink regulating the global atmospheric CO_2 concentration [5]. Unveiling the fundamental CO_2 carbonation chemistry is essential for facilitating carbon sequestration technologies, focusing on the link between carbonation efficiency and pH, salt type, and concentration [6, 7].

In the classical carbonation pathway of water-saturated conditions, converting atmospheric CO_2 to carbonate anion (CO_3^{2-}) is one of the prerequisites for the precipitation of carbonate minerals. When the conversion begins with CO_2 and water interactions, it subsequently involves the formation of carbonic acid (H_2CO_3) species, the deprotonation of H_2CO_3 and bicarbonate (HCO_3^-), which can be described by following the CO_2 hydration pathway [8, 9]:

$$\begin{aligned} CO_2(aq) + H_2O \rightleftharpoons H_2CO_3(aq) &\rightleftharpoons HCO_3^-(aq) + H^+ \\ &\rightleftharpoons CO_3^{2-}(aq) + 2H^+ \end{aligned} \quad (1)$$

The conversion of CO_2 to CO_3^{2-} can also initiate from the hydroxylation of CO_2 with the hydroxide ion (OH^-), followed by the deprotonation of HCO_3^-, as shown by the CO_2 hydroxylation pathway below [10, 11]:

$$CO_2(aq) + OH^- \rightleftharpoons HCO_3^-(aq) \rightleftharpoons CO_3^{2-}(aq) + H^+ \quad (2)$$

The conversion process and the equilibrium of these carbon-containing species in the aqueous solution are highly pH-dependent [7]. The thermodynamical equilibrium between CO_2 and HCO_3^- exists at pH of 6.4. H_2CO_3 and HCO_3^- anions establish the thermodynamical equilibrium at pH lower than 8.5. Prior experimental studies [7] indicate that when the pH surpasses 8.5, the reaction pathway eq. 2 takes precedence over the one outlined in eq. 1.

A molecular-level understanding of the formation of H_2CO_3 and HCO_3^-, and their dissociation is crucial to optimize CO_2 mineralization, such that many theoretical calculations, e.g., Density Functional Theory (DFT) calculations [12–15], *ab initio* molecular dynamics (AIMD) simulations [10, 16–18], and reactive molecular dynamics simulations [19–21] have been actively carried out. The energy barrier of H_2CO_3 formation significantly depends on the number of water molecules within the $CO_2{\cdot}nH_2O$ cluster. According to Nguyen et al. [12], the energy barrier of CO_2 hydration $CO_2 + nH_2O \rightleftharpoons H_2CO_3 + (n-1)H_2O$ decreases with the increasing number n of water molecules. When n increases from 1 to 3, the energy barrier of this reaction markedly decreases from $\sim$2.17 eV to $\sim$0.954 eV in aqueous solution at a temperature of 298 K. As more water molecules are involved in the reaction, a cyclic H-bonded network is formed via microsolvation, which lowers the energy barrier of proton transfers between water chains and CO_2. The optimum cyclic H-bonded water chain for CO_2 hydration requires three water molecules incorporated into the network, yielding a lower energy barrier

than the chain with two water molecules. In the static model simulations, when the water chain has more than three water molecules, further increasing water molecules no longer contributes to lowering the energy barrier of CO_2 hydration; instead, it even slightly increases the value [12, 18, 22]. Besides increasing water molecules, limiting the hydration space within a nanoconfinement also significantly enhances the formation of H_2CO_3 [21]. Likewise, adding water molecules also decreases the energy barrier of H_2CO_3 dissociation and decomposition [22–27]. When H_2CO_3 dissociation occurs with H_2O in the neutral solution, the HCO_3^-/H_3O^+ mixture can be stabilized only if H_3O^+ is solvated by a cluster of there water molecules [28]. Evidently, water molecules have catalytical effects on the formation of H_2CO_3 and its dissociation, which can be further enhanced by the interfacial carbonation of Ca/Mg minerals [3, 14, 29]. Regarding basic condition, the static model simulation shows that H_2CO_3 favors reacting with OH^- ions over water molecules for dissociation, forming CO_3^{2-} by a two-step mechanistic scheme [22].

HCO_3^- is critical to the nucleation of calcium carbonate, serving as a structural constituent in its formation [30]. The presence of HCO_3^- is sufficient to form calcium carbonate through the reaction $Ca^{2+} + 2HCO_3^- \rightleftharpoons CaCO_3 + CO_2 + H_2O$ [31]. By contrast with eq. 1 for which an intermediate step is required, HCO_3^- formation in eq. 2 is a straightforward reaction with CO_2 and OH^- as reactants. The CO_2 conversion pathway of eq. 2 has not been given enough attention [2, 4]. The formation of HCO_3^- through the reaction of CO_2 and OH^- is considered a predominant process in the basic solution [7, 32]. This reaction in the gas phase is energy-barrier-less, while it has a significant energy barrier in the aqueous solution [7, 26, 33]. The rise in the energy barrier of this reaction is attributed to the desolvation of the O atom in OH^- and the solvation of the O atom in CO_2 [33]. Once OH^- ion is consumed in this reaction, the basicity of the aqueous solution declines, which yields a different condition for the dissociation of HCO_3^-.

Although the hydration and dehydration of CO_2 in aqueous solutions have been discussed in many theoretical [9, 12, 16, 18, 21, 34] and experimental studies [7, 8, 35, 36], they still lack comprehensive understandings of the elementary processes on how the CO_3^{2-} anion and calcium carbonate ($CaCO_3$) are obtained from a series of progressive collective reactions. Particularly, most previous theoretical studies use static models and assume the reaction path of CO_2/H_2CO_3 with the nearby water molecules and/or OH^- ions [37, 38], which can significantly affect the molecular dynamics and free energy estimation for the reaction. Prior DFT-MD simulations [9, 16, 18, 39] have indicated the importance of solvent dynamics and statistical configuration ensembles in the H_2CO_3 formation. From this perspective, solvent dynamics are critical to all reactions along the conversion pathways described eq. 1 and 2.

Here, we investigate the complete carbonation pathways from CO_2 to CO_3^{2-} in the neutral and basic aqueous solutions using an enhanced sampling technique, i.e., well-tempered metadynamics [40, 41] in reactive molecular dynamics simulation [42, 43]. To achieve sufficient structural sampling and correctly evaluate energy barriers, sequential long metadynamics simulations ($>$ 5 ns each) are required to find the most probable pathway amongst many. Fig. 1 shows the workflow for the sequential metadynamics simulations. We progressively track the CO_2 hydration and deprotonation processes using a set of collective variables that can describe collective reaction behaviors of $CO_2/H_2O/OH^-$ mixtures, which allows us to distinguish how the carbonation reaction collectively and progressively happens in the system. The calcification path is identified after the formation of CO_3^{2-}. Unlike the static model simulation [12], we enable a sufficient sampling for the structural configurations of molecules in the system. The reactive simulations of these conversion reactions are implemented sequentially to provide the first atomistic insight into the complete carbonation pathways from CO_2 to $CaCO_3$.

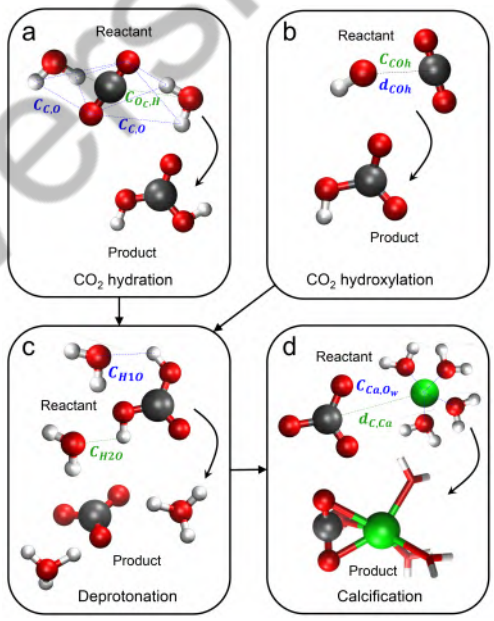

FIG. 1. Workflow of simulations implemented in this study and collective variables defined for each reaction. (a) CO_2 hydration, the coordination numbers of carbon atom C and oxygen atom O (C_{CO}) and the coordination number of carbon oxygen O_C and hydrogen (C_{OcH}) are defined for the reaction of CO_2 and H_2O. (b) CO_2 hydroxylation: the coordination number of C and OH^- (C_{COh}) and the distance the two species (d_{COh})are defined for the reaction of CO_2 and OH^-. (c) Deprotonation of H_2CO_3 and HCO_3^-: the coordination numbers of C_{H1O} and C_{H2O} are used in the proton transfer process; for the deprotonation of HCO_3^-, only the collective variable C_{H1O} is used. (d) Calcification: the coordination number of Ca and water oxygen (C_{Ca,O_w}) and the distance between C and Ca ($d_{C,Ca}$)) are used for the formation of $CaCO_3$ precursor. The definitions of these collective variables are described in the Methods Section.

II. METHODS

A. Simulation details

In this study, we consider the two chemical conditions for carbonation, i.e., the neutral and basic conditions as discussed here above. Therefore, we construct two bulk liquid models with a density of ~ 0.98 g/cm^3: the neutral solution model has 340 water molecules, and the basic solution model contains 1 Ca^{2+} cations and 2 OH^- ions. As a result, the two models are associated with the pH conditions at 7 and 13, respectively. All the carbonation reaction simulations are implemented in the NPT ensemble at 1 bar and 300 K. The pressure and temperature are controlled using the Nose-Hoover barostat and thermostat, respectively. The time integration is run in the Verlet algorithm with a timestep of 0.25 fs. The relaxation time for thermostating and barostating is set to 25 fs and 250 fs, respectively. All the systems are equilibrated for 1 ns before the production calculations. The reactive force field (ReaxFF) molecular dynamics simulation is performed using an in-house module of the LAMMPS package [44] (see details in II B). Given carbonation reactions are rare events in the atomistic scale within a limited time scale, we perform an enhanced sampling technique called well-tempered metadynamics simulations [45], from which we obtain the Free Energy Surface (FES) landscape for the carbonation reactions (see details in II C). The collective variables used for CO_2 hydration, CO_2 hydroxylation, deprotonation of H_2CO_3 and HCO_3^-, and calcification simulations are defined in Fig. 1 and II D.The FES is reconstructed by summing up all the Gaussian hills. We do not use any statistical reweighting method to build FES maps. We adopt the multidimensional lowest energy (MULE) path-searching algorithm [46] to find the minimum energy path in the FES. The well-tempered metadynamics simulations are implemented using an add-on package, i.e., PLUMED 2.5 [47] in LAMMPS. The VMD [48] package is used to visualize the trajectories.

B. Reactive molecular dynamics simulation

The carbonation process involves a series of chemical reactions. Herein, we perform ReaxFF molecular dynamics simulations to study the CO_2 hydration processes under neutral and basic conditions. ReaxFF is developed by training the atomistic structure and energy from quantum mechanics simulations[43, 49, 50]. The interatomic potential of this semi-empirical force field is cast within a bond-order formalism, which facilitates the description of the bond formation and breakage events in chemical reactions. The total potential energy (E_{total}) described in ReaxFF is defined as the sum of 5 components, namely the bonded (E_{bnod}), van der Waals (E_{vdw}), electrostatic (E_{qeq}), penalty ($E_{penalty}$), and overcoordination (E_{over}) interactions, expressed as follows:

$$E_{total} = E_{bnod} + E_{vdw} + E_{qeq} + E_{penalty} + E_{over} \qquad (3)$$

Previous studies [19–21] have shown the feasibility of ReaxFF molecular dynamics simulation in modeling carbonation reactions. Compared to DFT-based *ab initio* calculations, ReaxFF molecular dynamics simulations have lower computation expenses and enable the modeling of a larger molecular system [43]. To model the full carbonation reaction path, we adopt the ReaxFF potential developed by Pitman et al. [51]. The ReaxFF molecular simulation is performed using an in-house module of the Largescale Atomic/Molecular Massively Parallel Simulator (LAMMPS) package [44].

C. Well-tempered metadynamics simulation

It is well known that standard molecular dynamics simulation can get trapped in local energy minima, especially in complex energy landscapes, leading to inadequate exploration of the conformational space. This limitation restricts the ability to capture rare events with higher activation energy. Exploring large conformational spaces using standard molecular dynamics simulations can be computationally expensive, especially when trying to sample rare events. Simulating these events using brute force methods might require impractical time and computational resources. To this end, enhanced sampling methods offer advantages over standard molecular simulations by efficiently exploring complex energy landscapes, enabling the study of rare events. Here well-tempered metadynamics method is used to enhance the sampling of the ReaxFF molecular simulation. In this enhanced sampling method, an external bias $\tilde{V}(t,\xi)$ is added to the Hamiltonian:

$$\widetilde{V}(t,\xi) = \sum_{i=1}^{\left\lfloor \frac{t}{t_G} \right\rfloor} \omega \exp\left[-\frac{V(\xi,t)}{k_B \Delta T}\right] \exp\left[-\frac{\left|\xi^t - \xi^{i \bullet t_G}\right|^2}{2\sigma}\right] \qquad (4)$$

where ξ is the collective variable, ω and σ are the Gaussian height and width, t is time, t_G is the deposited time of hills, k_B represents the Boltzmann constant, and ΔT associates to the bias factor that controls the decrease rate of the Gaussian height $\omega \exp\left[-\frac{V(\xi,t)}{k_B \Delta T}\right]$. In the well-tempered metadynamics, the convergence of the Gaussian hills over time leads to a smoother convergence of the free energy landscape with respect to the standard metadynamics [40]. Apparently, the collective variable is essential and requires tracking the reactions since the bias potential is projected to this variable. The convergence test results for CO_2 hydration, CO_2 hydroxylation, deprotonation, and calcification are shown in Fig. S1. Note that noise still exists even after long runs, which is common when using well-tempered metadynamics in modeling chemical reactions [9, 21]. Since the energy difference of the MFEP profiles is already small within the last 1-2 ns, and the calculated energy values obtained here agree well with previous studies[18, 34], the simulations are considered converged.

D. Build collective variables

1. Collective variables of CO_2 hydration

For the CO_2 hydration process, we focus on two CO_2 hydration pathways: (a) $CO_2 + H_2O \rightarrow H_2CO_3$; (b) $CO_2 + OH^- \rightarrow HCO_3^-$. The formation of H_2CO_3 involves the formation of two new chemical bonds within a CO_2 molecule, i.e., an oxygen atom (O, from H_2O or OH^-) bonds to the carbon atom (C), and a hydrogen atom (H) bonds to the oxygen atom (Oc) of CO_2 molecule. Therefore, we build two collective variables (C_{CO}, C_{O_CH}) for the first reaction pathway to track the formation of H_2CO_3. C_{CO} is the coordination number of O atoms (from all H_2O molecules and/or OH^- ions) around the selected C atom, defined as:

$$C_{CO} = \sum_{k \in N_O} \frac{1 - \left(\frac{r_{\mathrm{CO}_k}}{r_0}\right)^m}{1 - \left(\frac{r_{\mathrm{CO}_k}}{r_0}\right)^n} \tag{5}$$

where r_{CO} is the C-O bond distance, r_0 represents the cutoff distance of C-O bond, r_0 = 2.0 Å, N_O is the total number of O atoms potentially participated in the reaction, m and n are two constant parameters of the switching function, m = 8, n = 16. Since O-H bond breakage and formation occur easily among water molecules and OH^- ions, all O atoms in the system can bond to the C atom. Hence, N_O includes all O atoms of water molecules in the neutral bulk model, and the O atoms of OH^- ions are also considered for the basic model. C_{O_CH} is the coordination number of H atoms around the Oc atom:

$$C_{O_CH} = \sum_{i \in N_{Oc}} \sum_{j \in N_H} \frac{1 - \left(\frac{r_{ij}}{r_c}\right)^m}{1 - \left(\frac{r_{ij}}{r_c}\right)^n} \tag{6}$$

where r_{ij} is the Oc-H bond distance, r_c is the cutoff distance of Oc-H bond, r_c = 1.3 Å, N_{Oc} and N_H are the total number of Oc and H atoms in the system, respectively, the constant parameters m and n use the same values as eq. (4). Therefore, the two collective variables can describe the collective CO_2 hydration behaviors in the system, with all water molecules and OH^- ions included. When the collective variables are at around 0, the bonds are not formed, while at about 1, it suggests that the bonds are formed.

The well-tempered metadynamics simulation protocols for CO_2 hydration reaction are as follows: the Gaussian height is set to 0.043 eV, and the Gaussian width for the coordination number is 0.05; the Gaussian hills are deposited for every 25 fs; the bias factor is set to 15. The total simulation time for the production is 10 ns, making the sampling sufficient in the phase space (see Fig. S2). A Gaussian width that is too small results in minor biases, slowing down the sampling process, whereas a width that is too large produces significant biases, potentially leading to inadequate sampling, particularly near saddle points. To find the optimum sampling, we performed several trial runs using different Gaussian widths, heights, basis factors, and hill deposition frequencies before our formal metadynamic simulations. It turned out that the values used above yielded the best sampling. The criteria is to have more crossing events. It turned out that the values used above yielded good sampling.

2. Collective variables of CO_2 hydroxylation

Let us now consider the collective variables for the second carbonation pathway, i.e., the straightforward reaction between CO_2 and OH^- ions in the basic condition. In this pathway, CO_2 hydration process happens straightforwardly between CO_2 molecules and OH^- ions with no need for H_2O dissociation, yielding HCO_3^-. Hence, the formation of HCO_3^- involves the formation of C-O bond only within a CO_2 molecule. To this end, we use the coordination number of the O atom in OH^- ions around the C atom as the first collective variable, i.e., C_{COh}:

$$C_{COh} = \sum_{k \in N_{Oh}} \frac{1 - \left(\frac{r_{COh_k}}{r_0}\right)^m}{1 - \left(\frac{r_{COh_k}}{r_0}\right)^n} \tag{7}$$

where r_{COh_k} is the distance between the C atom and O atom in OH^- ion (Oh), N_{Oh} is the total number of OH^- ions in the system, and the rest of the constant parameters are the same as eq. 4. In addition, we adopt the minimum distance between the selected C atom and OH^- ions as the second collective variable, i.e., d_{COh}. In order to obtain a variable with continuous derivatives, we define d_{COh} as:

$$d_{COh} = \frac{\beta}{\log\left(\sum_{k \in N_{Oh}} \exp\left(-\frac{\beta}{r_{COh_k}}\right)\right)} \tag{8}$$

where β is a self-specified constant, β = 10, N_{Oh} and r_{COh_k} represent the same physical meaning as eq. 4. To ensure that only OH^- ions meet the selected CO_2 molecule, we restrain the coordination number of Oh and hydrogen in water molecules at 0.

As an explanation, small C_{COh} values (near 0) and large d_{COh} values ($>$ 1.6 Å, see Fig. S2) indicate a reactant state, conversely large C_{COh} values (near 1) and small d_{COh} values (close to 1.7 Å) reflect the product state (HCO_3^-).

The well-tempered metadynamics simulation protocols for CO_2 hydroxylation reaction are as follows: the Gaussian height is set to 0.043 eV, and the Gaussian widths for the coordination number and distance are 0.05 and 0.1, respectively; the Gaussian hills are deposited for every 25 fs; the bias factor is set to 15; the production time is 10 ns.

3. Collective variables of deprotonation of H_2CO_3/HCO_3^-

In the complete carbonation pathway, H_2CO_3 and HCO_3^- are intermediate reaction products. CO_{32}^- is expected to be further produced from the deprotonation of these intermediate products for the precipitation of carbonate minerals. After the formation of H_2CO_3 and HCO_3^-, we implement free energy

calculations using the well-tempered metadynamics to the deprotonation of H_2CO_3 and HCO_3^- as already introduced in the last section. The deprotonation reaction is a proton transfer process from H_2CO_3/ HCO_3^- to water molecules or OH^- ions. A H_2CO_3 molecule has to lose two protons during the deprotonation. Therefore, we construct two collective variables (C_{H1O}, C_{H2O}) on the coordination number of the two protons (Hc) in H_2CO_3 and oxygen in the water molecules and OH^- ions, defined as follows:

$$C_{H1O} = \sum_{k \in N_O} \frac{1 - \left(\frac{r_{H_{C1}O_k}}{r_0}\right)^m}{1 - \left(\frac{r_{H_{c1}O_k}}{r_c}\right)^n} \tag{9}$$

$$C_{H2O} = \sum_{k \in N_O} \frac{1 - \left(\frac{r_{H_{C2}O_k}}{r_0}\right)^m}{1 - \left(\frac{r_{H_{C2}O_k}}{r_c}\right)^n} \tag{10}$$

where $r_{H_{C1}O_k}/r_{H_{C2}O_k}$ is the distance between the first/second H atom of H_2CO_3 and the k-th O atom of water molecules and OH^- ions, r_c is the cutoff distance for H-O bond, r_c = 1.3, N_O is the total number of O atoms in the system (except for oxygen in H_2CO_3), the constant parameters m and n are set to 8 and 16, respectively. Similar to the collective variables for CO_2 hydration, C_{H1O} and C_{H2O} involve all water molecules and OH^- ions in the system, making it possible to characterize the collective deprotonation behaviors. The small C_{H1O}/C_{H2O} numbers, close to 0, indicate an un-deprotonated state of H_2CO_3, whereas larger numbers, close to 1, correspond to a deprotonated state. Similarly, the deprotonation of HCO_3^- can also be tracked by the coordination number of HC. Since the HCO_3^- molecule has one proton only, we can simply use one collective variable C_{H1O} to characterize its deprotonation process.

In the well-tempered metadynamics simulations for the deprotonation of H_2CO_3 and HCO_3^-, we set the Gaussian height and width to 0.043 eV and 0.05, respectively. The time interval between two subsequent depositing Gaussian hills is 25 fs. The bias factor is set to 15. The entire simulation time is 12 ns.

4. *Collective variables of calcification*

For the most favorable reaction pathway of CO_3^{2-} formation, we observed that the CO_3^{2-} anion can be present stably in the presence of Ca^{2+} cation. We further investigate how the $CaCO_3$ precursor is formed. Free energy calculation for this calcification process is captured by the distance between C and Ca ($d_{C,Ca}$). To investigate the effect of water exchange on the first hydration shell of Ca, the coordination number Ow around of the Ca (C_{Ca,O_w}) is additionally used as the second collective variable:

$$C_{Ca,Ow} = \sum_{k \in N_{Ow}} \frac{1 - \left(\frac{r_{CaOw_k}}{r_0}\right)^m}{1 - \left(\frac{r_{CaOw_k}}{r_0}\right)^n} \tag{11}$$

where the r_{CaOw_k} is the distance between Ca and the k-th water oxygen, r_0 is the cutoff distance for Ca-Ow ionic bond, r_0 = 2.8, N_{Ow} is the total number of water oxygen in the system, m and n are 8 and 16, respectively.

For the well-tempered metadynamics implementation of this calcification process, we set the Gaussian height at 0.043 eV, the bias factor at 30, and the hill deposing frequency at 50 fs. The Gaussian widths for the distance and coordination number are 0.1 and 0.05, respectively. The simulation is run for 5 ns.

III. RESULTS AND DISCUSSION

A. CO_2 hydration and hydroxylation

Herein, we firstly focus on CO_2 hydration differences between neutral and basic conditions. In the neutral conditions, reactants for the CO_2 hydration reaction are simply CO_2 and H_2O molecules, following the first hydration pathway eq. 1. We construct two collective variables C_{CO} and C_{OcH} (C denotes the coordination number) to characterize the CO_2 hydration path for the well-tempered metadynamics simulations. Fig. 2a exhibits the FES landscape for the carbonation reaction between CO_2 and H_2O in neutral solution. Two local minimum energy states are distinguished on the FES landscape, labeled A and B, referring to reactants (CO_2 and H_2O) and product (H_2CO_3), respectively. As shown in Fig. S5a, the solvated CO_2 molecule is surrounded by around six water molecules in the first hydration shell, in agreement with the DFT-MD simulation [9]. The lowest reactant free energy state is located at the point C_{CO}=0.05, C_{OcH}=0.05. The small values of the two coordination numbers show that C and Oc atoms are weakly coordinated with Ow and Hw atoms of surrounding water molecules, indicating a solvation state of CO_2 molecule. However, the solvated CO_2 molecule is strongly hydrophobic with no hydrogen bond formed with these water molecules in the first hydration shell (see Fig. 2b) [18]. Along the minimum energy path, a Transitional State (TS) is observed. TS is at (C_{CO}=0.978,C_{OcH}=0.425), associating to a state where Ow is strongly coordinated to C and Hw is weakly coordinated to Oc, which indicates the formation of HCO_3^- before producing H_2CO_3. The snapshot in Fig. 2b illustrates the water attack process on CO_2 where a water molecule in the first hydration shell approaches C, and O-C-O angle is bending to form a C-Ow bond. Given that CO_2 is a nonpolar molecule, the O-C-O angle bending is primarily associated with hydrogen bonding interactions. Once the CO_2 gains dipole moment, the dipole-dipole interaction between the bent CO_2 and water molecule contributes to the formation of C-Ow bond (see Fig. 2b). In this collective reaction process, three water molecules participate in the hydration reaction: $CO_2 + 3H_2O \rightleftharpoons H_2CO_3 + 2H_2O$, which shows that the $CO_2 \cdot (H_2O)_3$ cluster yields the lowest free energy barrier for forming H_2CO_3, in good agreement with prior static model simulations [12, 16, 18, 52]. Protons are transferred among the $CO_2 \cdot (H_2O)_3$ cluster. The H_2CO_3 molecule has three conformers: *cis-trans*, *trans-trans*, and *cis-cis* [27, 53].

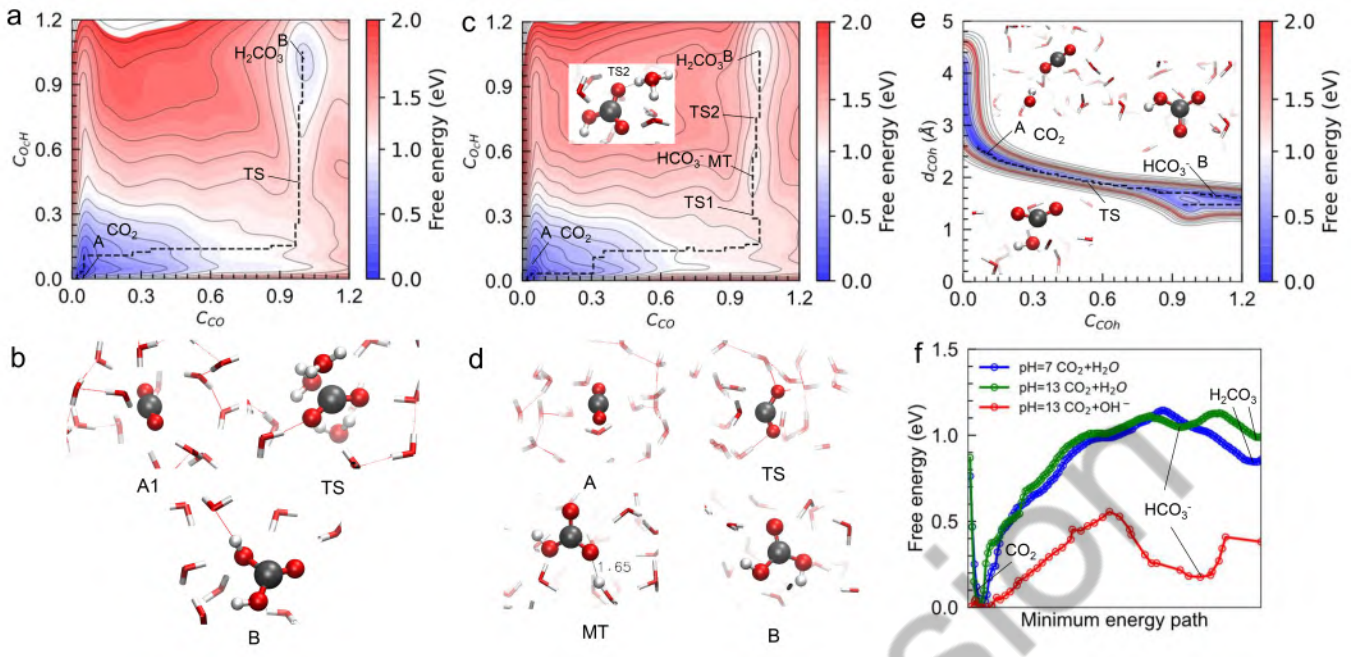

FIG. 2. FES of carbonation reactions in neutral (a) and basic (c, e) conditions. The snapshots in (b), (d), and (e) are associated with the FES of (a), (c), and (e), respectively. The dashed lines on the FES maps are the minimum energy path searched from MULE algorithm (see Methods). The minimum free energy profiles are shown in (f).

We observe these three H_2CO_3 conformers in the simulation (see Fig. S6), while the *trans-trans* and *cis-cis* conformers are prone to transform into the *cis-trans* conformer, which is mainly because the *cis-trans* conformer has the lowest free energy among the three conformers [9].

Then, we consider the CO_2 hydration process in the basic condition. The basic aqueous solution model includes CO_2, H_2O, Ca^{2+} and OH^-. Given that OH^- ions can participate in the association and dissociation reactions of H_2O molecules, we first investigate how the water complex and OH^- ions collectively react with the CO_2 molecule under the basic environment. Unlike the prior neutral case, oxygen and hydrogen atoms in OH^- ions are additionally taken into account for calculating C_{CO} and C_{OcH}, respectively. Doing so, the motion of molecules is out of constraint, enabling a collective reaction among CO_2, water complex, and OH^- ions. Fig. 2c depicts the FES of this collective reaction. Similar to the neutral case, we distinguish two free energy wells near the points (0, 0) and (1, 1), which are associated with the reactants (CO_2, H_2O, OH^-) and product (H_2CO_3), respectively. Apart from the two reactants and product states, we observe a third free energy well at the coordinate (0.971, 0.547), corresponding to a state where the C-Ow bond is strongly coordinated while the Oc-H bond is weakly coordinated. Hence, this well indicates the formation of HCO_3^- (see Fig. 2d). In this collective reaction, H_2CO_3 is formed through a stepwise mechanism consisting of two progressive reactions, i.e., $CO_2 + 2H_2O \rightleftharpoons HCO_3^- + H_3O^+$ and $HCO_3^- + H_3O^+ \rightleftharpoons H_2CO_3 + H_2O$. Interestingly, our simulation shows that the HCO_3^- formed in this collective reaction can be present in a metastable state in the basic condition, which differs from the neutral case. This metastable state has not been reported in previous static model simulations.

In essence, the CO_2 hydration processes shown in the basic and neutral solutions (see Fig. 2a, c) follow the same reaction, i.e., $CO_2 + H_2O \rightleftharpoons H_2CO_3$. HCO_3^- is simply an intermediate product along the CO_2 mineralization pathway. It is likely that the carbonation follows the hydroxylation pathway eq.(2) in the basic solution, starting from CO_2 hydroxylation reaction, i.e., $CO_2 + OH^- \rightleftharpoons HCO_3^-$. To this end, we construct the two collective variables (C_{COh}, d_{COh}) to track this selective reaction (see Fig. 1b). Note that only the OH^- ions are included in the basin, which ensures the CO_2 molecule reacts with OH^- ions only. Fig. 2e shows the FES of the reaction between CO_2 and OH^-. We identify the free energy wells related to the reactant and product, labeled A and B, respectively. The transitional state, marked TS, is at the point (0.612, 2.235). As illustrated in snapshots (Fig. 2e), the formation of HCO_3^- in this reaction follows a concerted mechanism. The O-C-O angle is bending due to the hydrogen bonding interactions, while the OH^- group is approaching the C atom at the transitional state, similar to that observed in the reaction between CO_2 and H_2O. This indicates that the angle bending is a prerequisite for the formation of the C-Ow/Oh bond [12, 16].

Up to now, we have examined three CO_2 hydration/hydroxylation pathways: path 1, CO_2 reacts with H_2O in a neutral condition; path 2, CO_2 reacts with H_2O in a basic condition; path 3, CO_2 reacts with OH^- in a basic condition. To compare the free energy barriers of the three cases mentioned above, we extract the minimum energy path from the FES landscape, as shown in Fig. 2f. The free energy barrier

for the formation of H_2CO_3 in the neutral and basic conditions are 1.144 eV and 1.126 eV, respectively. The basic condition merely yields a slight decrease in the energy barrier for the reaction of CO_2 and H_2O. The backward energy barrier for the basic condition is 0.137 eV, smaller than that of the neutral condition (0.299 eV), which means that the H_2CO_3 product is less thermodynamically stable in the basic solution than in the neutral condition. In contrast, the forward and backward free energy barrier for the reaction of CO_2 and OH^- are just 0.556 eV and 0.299 eV, respectively, significantly lower than that for the formation of H_2CO_3. Note that k_BT=0.0257 eV, in the basic condition, the system has significantly lower free energy when the CO_2 molecule reacts with OH^- than H_2O, meaning that this reaction yields a more thermodynamically stable state than the reaction of CO_2 and H_2O. The path 2 gives rise to the least thermodynamically stable system out of the three pathways. In this pathway, the reactive OH^- ions and H_2CO_3 molecule coexist in the system, making the system less energetically favorable. Instead, the path 3 consumes OH^- group and outputs HCO_3^-, yielding a more energetically favorable state than the path 2.

For the two CO_2 hydration reactions, there is no unique transition-state configuration. Instead, it differs for various initial water arrangements [18]. Note that the free energy barriers of the two reactions obtained from previous static model simulations could be significantly lower than the experiment values. Martirez et al. [18] calculated the forward activation energy of the reaction of CO_2 and nH_2O using various static model simulations. It turned out that the energy barriers were systematically lower than 0.8 eV and could be down to 0.24 eV as the number of water molecules increased to 9, which was markedly lower than the experiment value ($\sim$ 0.95 eV) [7]. Even though in some AIMD simulations [9, 25], the estimated activation barriers for this reaction were still slightly lower than the experiment value. Likewise, the forward energy barrier of the CO_2 hydroxylation reaction obtained from previous AIMD simulations was around 0.54 eV [10, 54], slightly underestimating the values compared with the experiment result of 0.585 eV at 298.15 K [37]. The discrepancy between the theoretical studies and experiments is due to insufficient structural sampling of solvent, according to Martirez et al. [18]. The static model simulations highly depend on the initial configurations of the reactants. Although the AIMD simulation considers the motion of molecules, given that it is computationally expensive, the structural sampling is still insufficient when the simulation time is limited. By contrast, our predicted energy barriers for the reactions of CO_2 hydration ($\sim$ 1.1 eV) and hydroxylation (0.556 eV) agree well with the experimental values, and the former predicted value is better than the static model simulation within the frame of water cluster (0.2-0.8 eV)[18]. Sufficiently long runs (10 ns) of our reactive molecular dynamics simulations effectively sample the collisions between reactants independent of the initial configurations.

B. Formation of CO_3^{2-}

Along the complete carbonation reaction pathways, the precipitation of carbonate minerals requires the basic ionic ingredients, i.e., carbonate anions (CO_3^{2-}) and metal cations (e.g., Ca^{2+} and Mg^{2+}). It is imperative to resolve the formation pathways of CO_3^{2-} under different solution environments. Following the CO_2 hydration and hydroxylation pathways discussed before, we then examine the subsequent deprotonation process of H_2CO_3 and HCO_3^-. Therefore, the deprotonation pathways examined include the following three conditions: path 1, deprotonation of H_2CO_3 in the neutral solution; path 2, deprotonation of H_2CO_3 in the basic solution ($Ca(OH)_2$); path 3, deprotonation of HCO_3^- in the basic solution ($(CaOH)^+$). Given that a single H_2CO_3 molecule has two protons, we use the two collective variables (C_{H1O}, C_{H2O}) to track its deprotonation process. While the HCO_3^- has one proton only, we adopt the C_{H1O} as the deprotonation reaction coordinate.

Fig. 3 presents the FES, minimum energy path, and snapshots for the three deprotonation pathways. For the first deprotonation pathway, we identified four free energy wells on the FES landscape, labeled A, B, and C (see Fig. 3a). We observed an asymmetric FES because the two protons have the same transferring probability. The state A is at the point (0.061, 0.054), indicating that the protons are still strongly attached to the H_2CO_3. When one of the two protons is lost from H_2CO_3, the system moves forward to state B, which corresponds to the reaction of forming HCO_3^- and hydronium ion (H_3O^+): $H_2CO_3 + H_2O \rightleftharpoons HCO_3^- + H_3O^+$ (see the snapshot in Fig. 3b). The transitional state of this deprotonation reaction is at the point (0.702, 0.043) or (0.047, 0.733), associating to a state where the distance between the donated proton and the acceptor is around 1.4 Å. When the left proton is further lost from the HCO_3^-, the system reaches state C, where the two protons are strongly coordinated to water molecules as the two collective variables are at large values (0.972, 0.981). The reaction of this process is written as: $HCO_3^- + H_2O \rightleftharpoons CO_3^{2-} + H_3O^+$.In the second deprotonation process, the distance between the donated proton and the oxygen acceptor is also around 1.4 Å. Our simulation suggests that the deprotonation of H_2CO_3 in the neutral condition is a two-step proton transfer process interacting with water molecules. The lost protons of H_2CO_3 cannot remain dangling alone in the aqueous. In this case, hydronium ions are formed (see Fig. 3b).

Fig. 3c depicts the deprotonation FES of H_2CO_3 in the basic solution. Note that there are still two OH^- ions in the system. Therefore, the two OH^- ions are also included in the basin for the calculation of C_{H1O} and C_{H2O}. Analogous to the first deprotonation pathway, the A, B, and C free energy wells are almost at the same position as Fig. 3a. Interestingly, we identify two extra free energy wells at the points (0.942, 0.201) and (0.198, 0.876), labeled D. When the system moves from B to D, the larger C_{HO} value remains while the small C_{HO} value slightly increases, indicating that the other proton is still attached on the HCO_3^-. From the trajectories, we observe that the water molecule is still the proton acceptor for

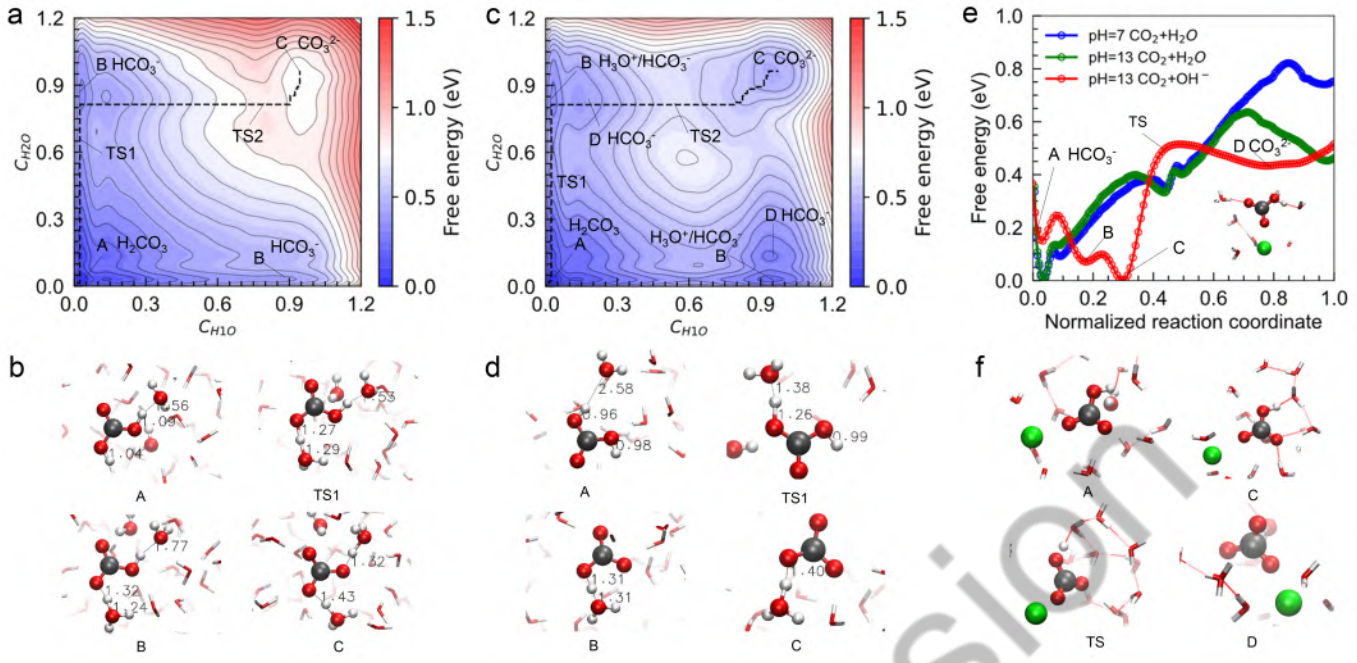

FIG. 3. FES of the deprotonation of H_2CO_3 in the neutral (a) and basic (c) conditions. (c) shows the FES for the deprotonation of HCO_3^- in the basic condition, together with the free energy profile along the minimum energy path in (a) and (c). The snapshots in (b), (d), and (f) are associated with the FES of (a), (c), and (e), respectively. The inset in (e) shows the snapshot of state B marked on the red curve.

the first deprotonation of H_2CO_3, though OH^- ions coexist in the solution (see Fig. 3d). Therefore, the state B labeled in Fig. 3c represents the formation of HCO_3^- and H_3O^+, identical to the case in Fig. 3a. Consequently, one notes that the solution is mixed with HCO_3^-, H_3O^+, OH^-, and H_2O at state B of the basic condition. Before the last proton is dissociated from HCO_3^-, we observe an intermediate reaction between H_3O^+ and OH^-: $H_3O^+ + OH^- \rightleftharpoons 2H_2O$. Hence, the transition between state B and state D is associated with the recombination of H_3O^+ and OH^-. Nevertheless, H_2O is still the proton acceptor for the deprotonation of HCO_3^-.The collective deprotonation reactions observed here are different from the previous static model simulation of Zhu et al. [22], who show that H_2CO_3 are always favorable to react with the surrounding OH^- ions and H_3O^+ ion formation is unlikely to occur. In our view, the discrepancy is still ascribed to the insufficient structural sampling in static model simulations. When the initial configurations of OH^- ions are close to the H_2CO_3 molecule, the two species are always prone to react with each other in the static model simulations. As a result, the water molecules act as spectators.

Fig. 3e shows the FES of HCO_3^- deprotonation in the third pathway, together with the free energy profiles along the minimum energy path for the first and second pathways. The first free energy well labeled A represents the reactant state (HCO_3^-) where the proton H_{CO_2} is strongly coordinated to the carbon oxygen and water molecules are far away from the HCO_3^- anion without forming hydrogen bonds. Apart from state A, there are two additional free energy wells (B and C) before the deprotonation state D, where the H_{CO_2} atom is weakly coordinated to a surrounding water molecule (see the inset of Fig. 3e and Fig. 3f). Two and three hydrogen bonds are formed between the HCO_3^- and the surrounding H_2O molecules in state B and C, respectively, which stabilizes the HCO_3^- and yields a lower free energy than the state A. In the third pathway, only one proton transfer happens between HCO_3^- and H_2O, making the deprotonation much easier than the other two pathways. This has the lowest free energy barrier out of the three pathways, only 0.515 eV. In contrast, the free energy barriers of H_2CO_3 deprotonation in the neutral and basic solutions are 0.822 eV and 0.636 eV. Note that the energy barrier for a single deprotonation reaction is similar among the three cases. The energy barriers of the first deprotonation in the neutral and basic cases are 0.382 eV and 0.399 eV, respectively, and that of the second deprotonation in the two cases are 0.473 eV and 0.304 eV, respectively, which are close to the energy barrier estimated for the third deprotonation pathway. As one can see from Fig. 3f, the Ca^{2+} cation is always near the HCO_3^- since one OH^- ion is consumed during the CO_2 hydroxylation reaction, which makes the Ca^{2+}-HCO_3^- and Ca^{2+}-CO_3^{2-} ion pairs formed easily along this carbonation pathway.

C. Estimation of the most favorable reaction path

We have identified the reaction pathways for the CO_2 hydration and H_2CO_3/HCO_3^- deprotonation process in the neutral and basic conditions. Consequently, CO_3^{2-} is formed through the sequential reactions. Herein, we summarize the complete carbonation pathways for the three cases, as shown

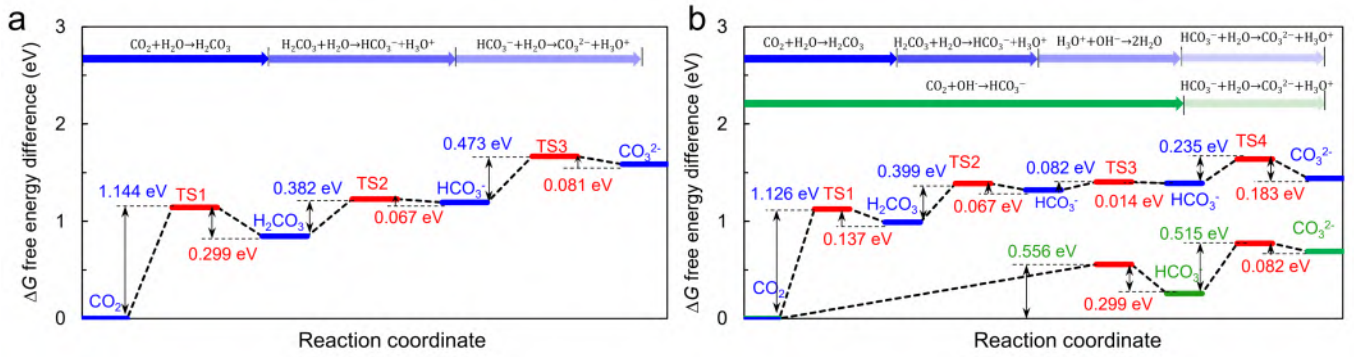

FIG. 4. Full conversion pathways from CO_2 to CO_3^{2-} in the neutral (a) and basic (b) aqueous solutions.

in Fig. 4. In the first carbonation pathway for the neutral solution, three progressive reactions are resolved. Note that the first reaction between CO_2 and H_2O in this carbonation pathway involves three water molecules instead of one. Water dissociation and association reactions occur among the three water molecules during the formation of H_2CO_3. Fig. 4b shows the complete collective CO_2 hydration pathway (blue) in the basic solution. Compared with the neutral solution, this carbonation pathway is more complicated, with extra reactions found during the CO_2 hydration and H_2CO_3 deprotonation processes. Fig. 4b also depicts the CO_2 hydroxylation pathway (green) in the basic environment where CO_2 reacts straightforwardly with OH^-. Hence, the formation of CO_3^{2-} in the pathway simply comprises two reactions.

The comparisons of the complete carbonation pathways in Fig. 4 indicate that the CO_2 hydroxylation pathway (Fig. 4b) requires the least energy for the conversion from CO_2 to CO_3^{2-} out of the three pathways, only 0.772 eV. In contrast, the free energy barriers between CO_2 and CO_3^{2-} in the first (Fig. 4a) and the second (Fig. 4b) CO_2 hydration pathways are 1.667 eV and 1.639 eV, showing less energetically favorable than the CO_2 hydroxylation pathway. However, collectively, CO_2 seems to be more likely to react with H_2O rather than OH^- in the basic aqueous solution according to the free energy profile of the second pathway. Such discrepancy is perhaps due to the enhanced sampling of metadynamics. To this end, we can roughly estimate the reaction rates of CO_2 hydration and CO_2 hydroxylation reactions using the Arrhenius equation (details can be found in Appendix):

$$k = Z_{AB}\rho \exp\left(\frac{-\Delta G}{RT}\right) \tag{12}$$

where Z_{AB} is the collision frequency of the reactants related to the number of reactants N_A and N_B, ρ is the steric factor, R is the gas constant, and ΔG is the activation energy. Then the reaction rate ratio of CO_2 hydroxylation (k_3) and CO_2 hydration (k_2) can be roughly expressed as $\frac{k_3}{k_2} \sim \frac{N_{OH^-}}{N_{H_2O}} \exp\left(\frac{\Delta G_2 - \Delta G_3}{RT}\right)$. Knowing the free energy barriers of the two reactions, we have $\frac{k_3}{k_2} \sim \frac{N_{OH^-}}{N_{H_2O}} \times 10^9$. It means that when the two reactions have the same reaction rate, the number of water molecules should be at least 10^9 times larger than the number of OH^- ions, which is impossible. Therefore, we can conclude that the third reaction pathway is the most favorable carbonation path.

Along each carbonation pathway, the first reaction always has the highest energy barrier, showing that forming a C-O bond is the rate-limiting process. The product CO_3^{2-} has markedly higher energy than other local minimum energy states, especially in the first pathway, so it is perhaps highly unstable. To this end, we further equilibrate the system at the product state. It turns out that the CO_3^{2-} formed in the first pathway retreats to the HCO_3^- state, while the CO_3^{2-} in the other two pathways remains stable. One notes that the backward energy barrier for CO_3^{2-} to HCO_3^- in the neutral case is just 0.081 eV because of the coexistence of CO_3^{2-} and H_3O^+, which allows the backward reaction to occur easily.

D. Formation of Ca_2^+-CO_3^{2-} ion pair

The CO_3^{2-} formed in the third pathway is stably present in the presence of Ca^{2+}. We further investigate how the $CaCO_3$ precursor is formed in this pathway. Fig. 5a shows the FES of the calcification process, and Fig. 5b depicts the free energy profile along the minimum energy path. To show the water exchange effect on the solvation of Ca^{2+} during the calcification, we use the coordination number of Ca^{2+} by water oxygen to capture the solvation state of Ca^{2+} [55]. As depicted in Fig. 5b, the free energy barriers of the calcification are markedly lower than any other reactions of the complete carbonation pathway. The main transitional state (TS1) for the calcification is between the swimming state A and the attaching state B (see the insets in Fig. 5a), where the CO_3^{2-} is heading to the solvated Ca^{2+} (with six water molecules in the first solvation shell) at the distance of around 4.3 Å. The free energy barrier of this transition is just 0.21 eV. As the two counterparts are approaching each other, the Ca^{2+} loses one water molecule from its solvation shell. The least energy state is the $CaCO_3{\cdot}5H_2O$ complex at state D where the C-Ca distance is around 2.8 Åand the Ca^{2+} is solvated by five water molecules and one oxygen atom of the CO_3^{2-} anion (see Fig. 5b), showing that the early calcification process is exergonic, consistent with the molecular dynamics simulation using a shell model for the calcium carbonate [34]. The $CaCO_3{\cdot}4H_2O$ complex at

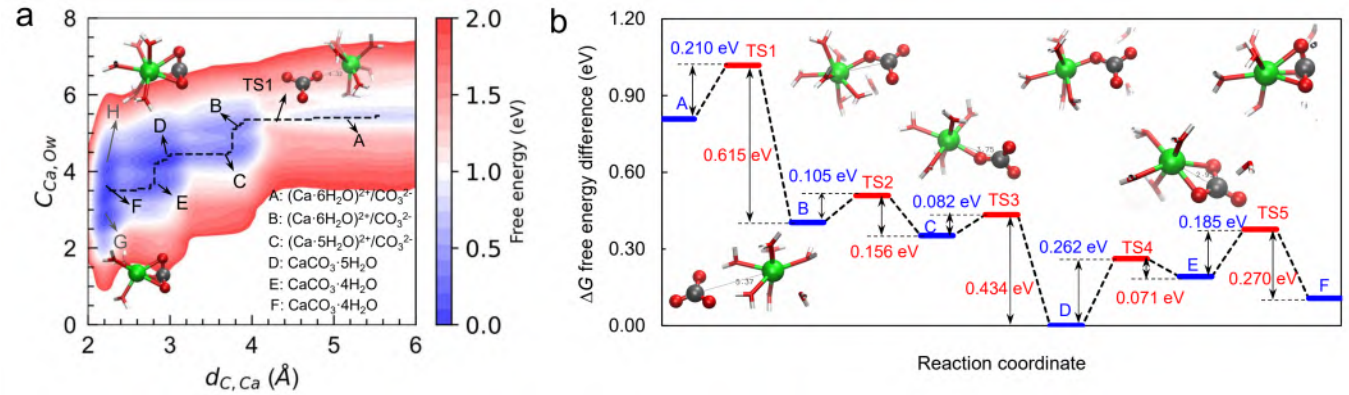

FIG. 5. Reactive metadynamics simulation for $CaCO_3$ formation. (a) The FES of calcification in basic solution after the carbonate anion is formed from the most favorable pathway. (b) The minimum energy path of the calcification reaction.

E is a metastable state where two carbon oxygens are coordinated to Ca^{2+}, and the Ca^{2+} is on the plane of CO_3^{2-}. It is possible that the C and Ca further approach at around 2.2 Å, causing the Ca^{2+} shifts toward the top of the CO_3^{2-} plane, and the three oxygens in CO_3^{2-} are coordinated to the Ca^{2+}. Since the calcification is a barrierless reaction, the two species can easily bond together when they coexist in the system, even in the standard molecular dynamics simulation.

Our results show that the CO_2 captured in the basic solutions can remain stable as CO_3^{2-}, especially in the presence of a counterpart like Ca^{2+}. Basic aqueous conditions are common in nature. For example, the pH of ocean is around 8.1 [56], and it includes abundant cations e.g., Mg^{2+}, Ca^{2+}, and Na^+, etc. It means that the ocean can be functionalized as a carbon sink. The basic condition of the ocean enables it to uptake atmospheric CO_2 molecules and, most importantly, to store them in forms of CO_3^{2-} or HCO_3^-. Especially the presence of Mg^{2+} and Ca^{2+} makes it even more favorable. The basic condition is also frequently seen in the pore solutions of concrete and natural minerals. Due to the continuous hydration reactions of cement, the concrete pore solution is usually in highly alkali conditions with a pH ranging from 12.3 $\sim$ 13.8 [57]. From our results, we can fairly deduce that carbonation reactions can happen in cement concrete. The long-term exposure of concrete to the atmosphere makes the concrete a carbon sink [58]. It is, therefore, important to consider the effect of basicity when evaluating the global carbon cycle.

IV. CONCLUSION

In this work, we use reactive simulation with metadynamics techniques to unveil the complete pathways (from CO_2 to the Ca_2^+-CO_3^{2-} ion pair) and collective reaction behaviors of carbonation reactions in neutral and basic solutions. The collective reaction behaviors of molecules in the processes of CO_2 hydration and hydroxylation, H_2CO_3/HCO_3^- deprotonation and calcification, are well captured by our collective variables. The collective and constrained samplings allow us to distinguish the different reaction pathways of carbonation. Our main conclusions are summarized as follows:

(1) We stress the importance of structural sampling for all the reactions along the complete carbonation pathways. Enhanced sampling with multiple crossing of the energy barriers is necessary to determine accurately the reaction energy barrier, in contrast with static models or dynamic models with single events, which are often used.

(2) The energy barriers of CO_2 with OH^- are much lower than with H_2O, yielding a faster reaction rate (10^9 higher at the same concentration). Thus, for the CO_2 speciation, a basic aqueous solution is critical to increase the reaction rate. This is because the CO_3^{2-} anion is most likely to form from the CO_2 hydroxylation pathway in a basic solution.

(3) When the CO_3^{2-} anion is formed in the basic solution, the calcification of $CaCO_3$ occurs with a markedly low free energy barrier. In contrast, forming CO_3^{2-} in the neutral bulk water is less thermodynamically favorable than that in the basic solution. We could infer a reasonable scenario for the full carbonation path of an alkali-earth solution: a CO_2 molecule speciates through the CO_2 hydroxylation pathway, then binds with an alkali-earth cation with a fast reaction rate.

Appendix A: Supplementary Materials

The Supplementary Information (SI) includes supplementary text and supplementary figures.

ACKNOWLEDGMENTS

This project was supported by the LabEx NUMEV (ANR-10-LABX-0020) within the I-Site MUSE (ANR-16-IDEX-0006). This work was performed using HPC resources from GENCI/TGCC clusters (2023 Grants AD010914034 and AD010914225)

[1] S. *Snbjrnsdttir*, B. Sigfússon, C. Marieni, D. Goldberg, S. R. Gislason, and E. H. Oelkers, Nature Reviews Earth & Environment **1**, 90 (2020).

[2] G. Gadikota, Nature Reviews Chemistry **4**, 78 (2020).

[3] Q. R. S. Miller, D. A. Dixon, S. D. Burton, E. D. Walter, D. W. Hoyt, A. S. McNeill, J. D. Moon, K. S. Thanthiriwatte, E. S. Ilton, O. Qafoku, C. J. Thompson, H. T. Schaef, K. M. Rosso, and J. S. Loring, The Journal of Physical Chemistry C **123**, 12871 (2019).

[4] M. J. Abdolhosseini Qomi, Q. R. S. Miller, S. Zare, H. T. Schaef, J. P. Kaszuba, and K. M. Rosso, Nature Reviews Chemistry **6**, 598 (2022).

[5] N. Gruber, D. C. E. Bakker, T. DeVries, L. Gregor, J. Hauck, P. Landschützer, G. A. McKinley, and J. D. Müller, Nature Reviews Earth & Environment **4**, 119 (2023).

[6] B. R. W. Pinsent and F. J. W. Roughton, Transactions of the Faraday Society **47**, 263 (1951).

[7] X. Wang, W. Conway, R. Burns, N. McCann, and M. Maeder, The Journal of Physical Chemistry A **114**, 1734 (2010).

[8] K. Adamczyk, M. Prémont-Schwarz, D. Pines, E. Pines, and E. T. J. Nibbering, Science **326**, 1690 (2009).

[9] D. Polino, E. Grifoni, R. Rousseau, M. Parrinello, and V.-A. Glezakou, The Journal of Physical Chemistry A **124**, 3963 (2020).

[10] K. Leung, I. M. B. Nielsen, and I. Kurtz, The Journal of Physical Chemistry B **111**, 4453 (2007).

[11] T. Zelovich, C. Simari, I. Nicotera, D. R. Dekel, and M. E. Tuckerman, Journal of Materials Chemistry A **10**, 11137 (2022).

[12] M. T. Nguyen, M. H. Matus, V. E. Jackson, V. T. Ngan, J. R. Rustad, and D. A. Dixon, The Journal of Physical Chemistry A **112**, 10386 (2008).

[13] J. Baltrusaitis and V. H. Grassian, The Journal of Physical Chemistry A **114**, 2350 (2010).

[14] A. Funk and H. F. R. Trettin, Industrial & Engineering Chemistry Research **52**, 2168 (2013).

[15] B. Wang and Z. Cao, Journal of Computational Chemistry **34**, 372 (2013).

[16] G. A. Gallet, F. Pietrucci, and W. Andreoni, Journal of Chemical Theory and Computation **8**, 4029 (2012).

[17] E. Grifoni, G. Piccini, and M. Parrinello, Proceedings of the National Academy of Sciences of the United States of America **116**, 4054 (2019), hn5ri Times Cited:6 Cited References Count:30.

[18] J. M. P. Martirez and E. A. Carter, Journal of the American Chemical Society **145**, 12561 (2023).

[19] S. Zare and M. J. A. Qomi, Physical Chemistry Chemical Physics **23**, 23106 (2021).

[20] S. Zare, A. Funk, and M. J. Abdolhosseini Qomi, The Journal of Physical Chemistry C **126**, 11574 (2022).

[21] N. Dasgupta, T. A. Ho, S. B. Rempe, and Y. Wang, The Journal of Physical Chemistry Letters **14**, 1693 (2023).

[22] J. Zhu, D. Shen, B. Jin, and S. Wu, Construction and Building Materials **342**, 128000 (2022).

[23] T. Loerting, C. Tautermann, R. T. Kroemer, I. Kohl, A. Hallbrucker, E. Mayer, and K. R. Liedl, Angewandte Chemie International Edition **39**, 891 (2000).

[24] C. S. Tautermann, A. F. Voegele, T. Loerting, I. Kohl, A. Hallbrucker, E. Mayer, and K. R. Liedl, Chemistry – A European Journal **8**, 66 (2002).

[25] A. Stirling and I. Pápai, The Journal of Physical Chemistry B **114**, 16854 (2010).

[26] A. Stirling, The Journal of Physical Chemistry B **115**, 14683 (2011).

[27] M. Galib and G. Hanna, The Journal of Physical Chemistry B **115**, 15024 (2011).

[28] M. Galib and G. Hanna, The Journal of Physical Chemistry B **118**, 5983 (2014).

[29] S. M. Mutisya and A. G. Kalinichev, "Carbonation reaction mechanisms of portlandite predicted from enhanced ab initio molecular dynamics simulations," (2021).

[30] Y.-C. Huang, A. Rao, S.-J. Huang, C.-Y. Chang, M. Drechsler, J. Knaus, J. C. C. Chan, P. Raiteri, J. D. Gale, and D. Gebauer, Angewandte Chemie International Edition **60**, 16707 (2021).

[31] M. A. Torres, A. J. West, and G. Li, Nature **507**, 346 (2014).

[32] T. H. Maren, Annual Review of Physiology **50**, 695 (1988).

[33] K. Iida, D. Yokogawa, H. Sato, and S. Sakaki, Chemical Physics Letters **443**, 264 (2007).

[34] G. A. Tribello, F. Bruneval, C. Liew, and M. Parrinello, The Journal of Physical Chemistry B **113**, 11680 (2009).

[35] T. Mori, K. Suma, Y. Sumiyoshi, and Y. Endo, The Journal of Chemical Physics **134**, 044319 (2011).

[36] X. Wang and T. Bürgi, Angewandte Chemie International Edition **60**, 7860 (2021).

[37] Z. Peng and J. Merz, Kenneth M., Journal of the American Chemical Society **114**, 2733 (1992).

[38] M. J. Loferer, C. S. Tautermann, H. H. Loeffler, and K. R. Liedl, Journal of the American Chemical Society **125**, 8921 (2003).

[39] P. P. Kumar, A. G. Kalinichev, and R. J. Kirkpatrick, The Journal of Physical Chemistry B **113**, 794 (2009).

[40] A. Laio and M. Parrinello, Proceedings of the National Academy of Sciences of the United States of America **99**, 12562 (2002).

[41] A. Barducci, G. Bussi, and M. Parrinello, Physical Review Letters **100**, 020603 (2008).

[42] A. C. T. van Duin, S. Dasgupta, F. Lorant, and W. A. Goddard, The Journal of Physical Chemistry A **105**, 9396 (2001).

[43] T. P. Senftle, S. Hong, M. M. Islam, S. B. Kylasa, Y. Zheng, Y. K. Shin, C. Junkermeier, R. Engel-Herbert, M. J. Janik, H. M. Aktulga, T. Verstraelen, A. Grama, and A. C. T. van Duin, npj Computational Materials **2**, 15011 (2016).

[44] A. P. Thompson, H. M. Aktulga, R. Berger, D. S. Bolintineanu, W. M. Brown, P. S. Crozier, P. J. in 't Veld, A. Kohlmeyer, S. G. Moore, T. D. Nguyen, R. Shan, M. J. Stevens, J. Tranchida, C. Trott, and S. J. Plimpton, Computer Physics Communications **271**, 108171 (2022).

[45] M. Bonomi, A. Barducci, and M. Parrinello, Journal of Computational Chemistry **30**, 1615 (2009).

[46] H. Fu, H. Chen, X. Wang, H. Chai, X. Shao, W. Cai, and C. Chipot, Journal of Chemical Information and Modeling **60**, 5366 (2020).

[47] G. A. Tribello, M. Bonomi, D. Branduardi, C. Camilloni, and G. Bussi, Computer Physics Communications **185**, 604 (2014).

[48] W. Humphrey, A. Dalke, and K. Schulten, Journal of Molecular Graphics **14**, 33 (1996).

[49] A. C. T. van Duin, A. Strachan, S. Stewman, Q. S. Zhang, X. Xu, and W. A. Goddard, Journal of Physical Chemistry A **107**, 3803 (2003), 678yh Times Cited:559 Cited References Count:44.

[50] H. Manzano, S. Moeini, F. Marinelli, A. C. van Duin, F. J. Ulm, and R. J. Pellenq, Journal of the American Chemical Society **134**, 2208 (2012), manzano, Hegoi Moeini, Sina Marinelli, Francis van Duin, Adri C T Ulm, Franz-Josef Pellenq, Roland J-M eng Research Support, U.S. Gov't, Non-P.H.S. J Am Chem Soc. 2012 Feb 1;134(4):2208-15. doi: 10.1021/ja209152n. Epub 2012 Jan 20.

[51] M. C. Pitman and A. C. T. van Duin, Journal of the American Chemical Society **134**, 3042 (2012).

[52] R. Dupuis, R. Pellenq, J.-B. Champenois, and A. Poulesquen, The Journal of Physical Chemistry C **124**, 8288 (2020).

[53] T. Loerting and J. Bernard, ChemPhysChem **11**, 2305 (2010).

[54] Z. Peng and J. Merz, Kenneth M., Journal of the American Chemical Society **115**, 9640 (1993).

[55] M. Kellermeier, P. Raiteri, J. K. Berg, A. Kempter, J. D. Gale, and D. Gebauer, ChemPhysChem **17**, 3535 (2016).

[56] H. C. Wu, D. Dissard, E. Douville, D. Blamart, L. Bordier, A. Tribollet, F. Le Cornec, E. Pons-Branchu, A. Dapoigny, and C. E. Lazareth, Nature Communications **9**, 2543 (2018).

[57] A. Vollpracht, B. Lothenbach, R. Snellings, and J. Haufe, Materials and Structures **49**, 3341 (2016).

[58] F. Xi, S. J. Davis, P. Ciais, D. Crawford-Brown, D. Guan, C. Pade, T. Shi, M. Syddall, J. Lv, L. Ji, L. Bing, J. Wang, W. Wei, K.-H. Yang, B. Lagerblad, I. Galan, C. Andrade, Y. Zhang, and Z. Liu, Nature Geoscience **9**, 880 (2016).